Research Article | Vol. 24, No. 22 | 31 Oct 2016 | OPTICS EXPRESS A1306

Optics EXPRESS

Maximal absorption regime in random media

VOLODYMYR B. KOMAN, CHRISTIAN SANTSCHI,* AND OLIVIER J. F. MARTIN

Nanophotonics and Metrology Laboratory (NAM), Swiss Federal Institute of Technology (EPFL), 1015 Lausanne, Switzerland

*christian.santschi@epfl.ch

www.nanophotonics.ch

Abstract: Efficient optical energy transfer is key to many technologies, ranging from biosensing to photovoltaics. Here, for the first time we show that by introducing a random medium with appropriate filling factor, absorption in a specific volume can be maximized. Using both numerical simulations and an analytical diffusion model, we identify design rules to maximize absorption in the system with different geometrical and scattering properties. By combining a random medium with an open photonic cavity, we numerically demonstrate a 23-fold enhancement of the absorbed energy. We also show how absorption as high as 99% can be reached in a device as thin as 500 μm for normal incidence illumination. Finally, our data indicate that introducing a non-absorbing random medium into a light trapping system for thin solar cells can enhance absorption of energy by a factor of 2.2. This absorption enhancement, caused by the random medium, is broadband and wide-angle and can help design efficient solar cells, light trapping devices, biosensors and random lasers.

OCIS codes: (260.2710) Inhomogeneous optical media; (290.4210) Multiple scattering; (300.1030) Absorption; (040.5350) Photovoltaic; (310.6845) Thin film devices and applications; (140.3945) Microcavities.

References and links

1. D. S. Wiersma, P. Bartolini, A. Lagendijk, and R. Righini, "Localization of light in a disordered medium," Nature **390**(6661), 671–673 (1997).
2. M. Störzer, P. Gross, C. M. Aegerter, and G. Maret, "Observation of the critical regime near Anderson localization of light," Phys. Rev. Lett. **96**(6), 063904 (2006).
3. D. S. Wiersma, "Disordered photonics," Nat. Photonics **7**(3), 188–196 (2013).
4. D. S. Wiersma and A. Lagendijk, "Light diffusion with gain and random lasers," Phys. Rev. E Stat. Phys. Plasmas Fluids Relat. Interdiscip. Topics **54**(4), 4256–4265 (1996).
5. H. Cao, Y. G. Zhao, S. T. Ho, E. W. Seelig, Q. H. Wang, and R. P. H. Chang, "Random Laser Action in Semiconductor Powder," Phys. Rev. Lett. **82**(11), 2278–2281 (1999).
6. H. Cao, "Lasing in random media," Waves Random Media **13**(3), R1–R39 (2003).
7. D. S. Wiersma, "The physics and applications of random lasers," Nat. Phys. **4**(5), 359–367 (2008).
8. I. M. Vellekoop, A. Lagendijk, and A. P. Mosk, "Exploiting disorder for perfect focusing," Nat. Photonics **4**, 320–322 (2010).
9. Y. Choi, T. R. Hillman, W. Choi, N. Lue, R. R. Dasari, P. T. C. So, W. Choi, and Z. Yaqoob, "Measurement of the time-resolved reflection matrix for enhancing light energy delivery into a scattering medium," Phys. Rev. Lett. **111**(24), 243901 (2013).
10. Z. Yaqoob, D. Psaltis, M. S. Feld, and C. Yang, "Optical phase conjugation for turbidity suppression in biological samples," Nat. Photonics **2**(2), 110–115 (2008).
11. S. M. Popoff, G. Lerosey, R. Carminati, M. Fink, A. C. Boccara, and S. Gigan, "Measuring the transmission matrix in optics: an approach to the study and control of light propagation in disordered media," Phys. Rev. Lett. **104**(10), 100601 (2010).
12. Y. D. Chong and A. D. Stone, "Hidden black: coherent enhancement of absorption in strongly scattering media," Phys. Rev. Lett. **107**(16), 163901 (2011).
13. T. Svensson, E. Adolfsson, M. Lewander, C. T. Xu, and S. Svanberg, "Disordered, strongly scattering porous materials as miniature multipass gas cells," Phys. Rev. Lett. **107**(14), 143901 (2011).
14. V. B. Koman, C. Santschi, and O. J. F. Martin, "Multiscattering-enhanced absorption spectroscopy," Anal. Chem. **87**(3), 1536–1543 (2015).
15. G. Suárez, C. Santschi, V. I. Slaveykova, and O. J. F. Martin, "Sensing the dynamics of oxidative stress using enhanced absorption in protein-loaded random media," Sci. Rep. **3**, 3447 (2013).
16. V. Koman, G. Suárez, C. Santschi, V. J. Cadarso, J. Brugger, N. von Moos, V. I. Slaveykova, and O. J. F. Martin, "A portable microfluidic-based biophotonic sensor for extracellular H_2O_2 measurements," Proc. SPIE **8572**, 857218 (2013).

#269763 http://dx.doi.org/10.1364/OE.24.0A1306
Journal © 2016 Received 4 Jul 2016; revised 28 Aug 2016; accepted 30 Aug 2016; published 7 Sep 2016

Optics EXPRESS

17. V. B. Koman, C. Santschi, N. R. von Moos, V. I. Slaveykova, and O. J. F. Martin, "Portable oxidative stress sensor: dynamic and non-invasive measurements of extracellular H_2O_2 released by algae," Biosens. Bioelectron. **68**, 245–252 (2015).
18. O. L. Muskens, J. G. Rivas, R. E. Algra, E. P. A. M. Bakkers, and A. Lagendijk, "Design of Light Scattering in Nanowire Materials for Photovoltaic Applications," Nano Lett. **8**(9), 2638–2642 (2008).
19. K. Vynck, M. Burresi, F. Riboli, and D. S. Wiersma, "Photon management in two-dimensional disordered media," Nat. Mater. **11**(12), 1017–1022 (2012).
20. F. Pratesi, M. Burresi, F. Riboli, K. Vynck, and D. S. Wiersma, "Disordered photonic structures for light harvesting in solar cells," Opt. Express **21**(S3 Suppl 3), A460–A468 (2013).
21. Y. Hamakawa, *Thin-Film Solar Cells: Next Generation Photovoltaics and its Applications*, Vol. 13 (Springer Science & Business Media, 2004).
22. A. Polman and H. A. Atwater, "Photonic design principles for ultrahigh-efficiency photovoltaics," Nat. Mater. **11**(3), 174–177 (2012).
23. S.-B. Rim, S. Zhao, S. R. Scully, M. D. McGehee, and P. Peumans, "An effective light trapping configuration for thin-film solar cells," Appl. Phys. Lett. **91**(24), 243501 (2007).
24. K. Tvingstedt, S. Dal Zilio, O. Inganäs, and M. Tormen, "Trapping light with micro lenses in thin film organic photovoltaic cells," Opt. Express **16**(26), 21608–21615 (2008).
25. Y. Zhou, F. Zhang, K. Tvingstedt, W. Tian, and O. Inganäs, "Multifolded polymer solar cells on flexible substrates," Appl. Phys. Lett. **93**(3), 033302 (2008).
26. S. D. Zilio, K. Tvingstedt, O. Inganäs, and M. Tormen, "Fabrication of a light trapping system for organic solar cells," Microelec. Eng. **86**(4-6), 1150–1154 (2009).
27. L. Song and A. Uddin, "Design of high efficiency organic solar cell with light trapping," Opt. Express **20**(S5 Suppl 5), A606–A621 (2012).
28. K. R. Catchpole and A. Polman, "Plasmonic solar cells," Opt. Express **16**(26), 21793–21800 (2008).
29. H. A. Atwater and A. Polman, "Plasmonics for improved photovoltaic devices," Nat. Mater. **9**(3), 205–213 (2010).
30. V. E. Ferry, J. N. Munday, and H. A. Atwater, "Design considerations for plasmonic photovoltaics," Adv. Mater. **22**(43), 4794–4808 (2010).
31. C. Cocoyer, L. Rocha, L. Sicot, B. Geffroy, R. de Bettignies, C. Sentein, C. Fiorini-Debuisschert, and P. Raimond, "Implementation of submicrometric periodic surface structures toward improvement of organic-solar-cell performances," Appl. Phys. Lett. **88**(13), 133108 (2006).
32. J. B. Kim, P. Kim, N. C. Pegard, S. J. Oh, C. R. Kagan, J. W. Fleischer, H. A. Stone, and Y.-L. Loo, "Wrinkles and deep folds as photonic structures in photovoltaics," Nat. Photonics **6**(5), 327–332 (2012).
33. Y. Yao, J. Yao, V. K. Narasimhan, Z. Ruan, C. Xie, S. Fan, and Y. Cui, "Broadband light management using low-Q whispering gallery modes in spherical nanoshells," Nat. Commun. **3**, 664 (2012).
34. P. Spinelli, M. A. Verschuuren, and A. Polman, "Broadband omnidirectional antireflection coating based on subwavelength surface Mie resonators," Nat. Commun. **3**, 692 (2012).
35. C. Battaglia, J. Escarre, K. Soderstrom, M. Charriere, M. Despeisse, F.-J. Haug, and C. Ballif, "Nanomoulding of transparent zinc oxide electrodes for efficient light trapping in solar cells," Nat. Photonics **5**(9), 535–538 (2011).
36. S. Basu Mallick, M. Agrawal, A. Wangperawong, E. S. Barnard, K. K. Singh, R. J. Visser, M. L. Brongersma, and P. Peumans, "Ultrathin crystalline-silicon solar cells with embedded photonic crystals," Appl. Phys. Lett. **100**(5), 053113 (2012).
37. Z. Tang, W. Tress, and O. Inganäs, "Light trapping in thin film organic solar cells," Mater. Today **17**(8), 389–396 (2014).
38. C. Rockstuhl, S. Fahr, K. Bittkau, T. Beckers, R. Carius, F. J. Haug, T. Söderström, C. Ballif, and F. Lederer, "Comparison and optimization of randomly textured surfaces in thin-film solar cells," Opt. Express **18**(S3), A335–A341 (2010).
39. D. Madzharov, R. Dewan, and D. Knipp, "Influence of front and back grating on light trapping in microcrystalline thin-film silicon solar cells," Opt. Express **19**(S2), A95–A107 (2011).
40. V. E. Ferry, M. A. Verschuuren, M. C. Lare, R. E. I. Schropp, H. A. Atwater, and A. Polman, "Optimized spatial correlations for broadband light trapping nanopatterns in high efficiency ultrathin film a-Si:H solar cells," Nano Lett. **11**(10), 4239–4245 (2011).
41. N. A. Bruce and J. T. Chalker, "Multiple scattering in the presence of absorption: a theoretical treatment for quasi one-dimensional systems," J. Phys. A **29**(14), 3761–3768 (1996).
42. S. F. Liew, S. M. Popoff, A. P. Mosk, W. L. Vos, and H. Cao, "Transmission channels for light in absorbing random media: From diffusive to ballistic-like transport," Phys. Rev. B **89**(22), 224202 (2014).
43. O. S. Ojambati, H. Yılmaz, A. Lagendijk, A. P. Mosk, and W. L. Vos, "Coupling of energy into the fundamental diffusion mode of a complex nanophotonic medium," New J. Phys. **18**(4), 043032 (2016).
44. R. Sarma, A. G. Yamilov, S. Petrenko, Y. Bromberg, and H. Cao, "Control of energy density inside a disordered medium by coupling to open or closed channels," Phys. Rev. Lett. **117**(8), 086803 (2016).
45. R. Rammal and B. Doucot, "Invariant imbedding approach to localization. I. General framework and basic equations," J. Phys. France **48**(4), 509–526 (1987).
46. V. Freilikher, M. Pustilnik, and I. Yurkevich, "Effect of absorption on the wave transport in the strong localization regime," Phys. Rev. Lett. **73**(6), 810–813 (1994).

Optics EXPRESS

47. P. Pradhan and N. Kumar, "Localization of light in coherently amplifying random media," Phys. Rev. B Condens. Matter **50**(13), 9644–9647 (1994).
48. A. Y. Zyuzin, "Weak localization in backscattering from an amplifying medium," Europhys. Lett. **26**(7), 517–520 (1994).
49. Z.-Q. Zhang, "Light amplification and localization in randomly layered media with gain," Phys. Rev. B Condens. Matter **52**(11), 7960–7964 (1995).
50. A. K. Gupta and A. M. Jayannavar, "Electron wave transport in coherently absorptive random media," Phys. Rev. B Condens. Matter **52**(6), 4156–4161 (1995).
51. A. Y. Zyuzin, "Transmission fluctuations and spectral rigidity of lasing states in a random amplifying medium," Phys. Rev. E Stat. Phys. Plasmas Fluids Relat. Interdiscip. Topics **51**(6), 5274–5278 (1995).
52. C. W. J. Beenakker, J. C. J. Paasschens, and P. W. Brouwer, "Probability of reflection by a random laser," Phys. Rev. Lett. **76**(8), 1368–1371 (1996).
53. J. C. J. Paasschens, T. S. Misirpashaev, and C. W. J. Beenakker, "Localization of light: dual symmetry between absorption and amplification," Phys. Rev. B Condens. Matter **54**(17), 11887–11890 (1996).
54. J. Heinrichs, "Light amplification and absorption in a random medium," Phys. Rev. B **56**(14), 8674–8682 (1997).
55. S. K. Joshi and A. M. Jayannavar, "Transmission and reflection from a disordered lasing medium," Phys. Rev. B **56**(19), 12038–12041 (1997).
56. P. K. Datta, "Transmission and reflection in a perfectly amplifying and absorbing medium," Phys. Rev. B **59**(16), 10980–10984 (1999).
57. X. Jiang and C. M. Soukoulis, "Transmission and reflection studies of periodic and random systems with gain," Phys. Rev. B **59**(9), 6159–6166 (1999).
58. S. Mujumdar, R. Torre, H. Ramachandran, and D. Wiersma, "Monte Carlo calculations of spectral features in random lasing," J. Nanophotonics **4**(1), 041550 (2010).
59. R. Uppu and S. Mujumdar, "Persistent coherent random lasing using resonant scatterers," Opt. Express **19**(23), 23523–23531 (2011).
60. E. Hecht and A. Zajac, "Optics Addison-Wesley," Reading, Mass, 301–305 (1974).
61. O. Mengual, G. Meunier, I. Cayré, K. Puech, and P. Snabre, "TURBISCAN MA 2000: multiple light scattering measurement for concentrated emulsion and suspension instability analysis," Talanta **50**(2), 445–456 (1999).
62. D. Toublanc, "Henyey-Greenstein and Mie phase functions in Monte Carlo radiative transfer computations," Appl. Opt. **35**(18), 3270–3274 (1996).
63. D. Contini, F. Martelli, and G. Zaccanti, "Photon migration through a turbid slab described by a model based on diffusion approximation. I. Theory," Appl. Opt. **36**(19), 4587–4599 (1997).
64. R. Sarma, A. Yamilov, S. F. Liew, M. Guy, and H. Cao, "Control of mesoscopic transport by modifying transmission channels in opaque media," Phys. Rev. B **92**(21), 214206 (2015).
65. S. F. Liew, J. Forster, H. Noh, C. F. Schreck, V. Saranathan, X. Lu, L. Yang, R. O. Prum, C. S. O'Hern, E. R. Dufresne, and H. Cao, "Short-range order and near-field effects on optical scattering and structural coloration," Opt. Express **19**(9), 8208–8217 (2011).
66. A. Kienle, "Light diffusion through a turbid parallelepiped," J. Opt. Soc. Am. A **22**(9), 1883–1888 (2005).
67. J. H. Karp, E. J. Tremblay, and J. E. Ford, "Planar micro-optic solar concentrator," Opt. Express **18**(2), 1122–1133 (2010).

1. Introduction

Light propagation in disordered optical materials has been extensively studied for Anderson localization [1–3], random lasers [4–7] and light focusing below the diffraction limit [8, 9]. Additionally, recent developments in adaptive wavefront shaping techniques have stimulated research on highly transmitting (or so-called open) channels in random media [10–12] and coherently enhanced absorption [12]. Elongated optical paths – present in random media – recently paved the way for new sensing applications: gas camera sensors [13], multiscattering-enhanced absorption spectroscopy [14] and multiscattering-enhanced optical probes [15–17]. Finally, random media offer the possibility to improve photovoltaic devices by enhancing their absorption and increasing the optical path of light [18–20]. The present manuscript is devoted to the latter direction.

Recent trends in photovoltaics suggest moving towards thin film solar cells, where the recombination losses of generated hole-electron pairs are minimized [21]. However, such trend also requires efficient light trapping methods to maximize absorption within a thin solar cell [22]. Existing light trapping schemes utilize geometric engineering [23–27], plasmonic nanoparticles [28–30], metallic and dielectric gratings [31, 32], resonant dielectric nanoparticles [33, 34] and photonic crystals [35–37]. Geometric engineering schemes and gratings can suffer from defects and often require alignment or a tracking system, whereas

Optics EXPRESS

nanoparticles and photonic crystals are resonant and do not necessarily cover the full solar spectrum [37]. In this context, random structures offer broadband and wide-angle performances, which is crucial in solar energy harvesting [19].

To date, random structures for light trapping applications include randomly textured patterns on the front or back side of solar cells [19, 38–41]. Interestingly, these works mainly focus on two dimensional structures. Furthermore, their performances are usually only evaluated in terms of structural correlations at a given filling factor in the strong localization regime: authors seek the optimal conditions, in which light can be efficiently coupled to the Anderson closed loops that provide high absorption. On the other hand, it was recently theoretically predicted that the so-called diffusive regime with moderate filling factors is also beneficial for absorption thanks to the formation of eigenchannels with long optical paths [42]. This concept is experimentally implemented using wavefront shaping techniques, demonstrating enhanced absorption in 3D media up to 7.4 times [43, 44]. However, this technique suffers from a serious limitation: it requires expensive and precise equipment to control the input channels.

Stimulated by these findings and using numerical simulations, we study three-dimensional random media in an absorbing background with varying filling factors, ranging from a homogenous medium to a diffusion-like and, finally, to a close-packed random medium. In that context, we should acknowledge a vast number of theoretical works that studied reflection and transmission of light in random media with absorption or gain [45–57]. In contrast to those previous studies, we find that for a given geometrical configuration, the absorbed energy reaches its maximum at a specific mean free path. As discussed above, most of the previous studies concentrated on the strong scattering regime, while the effect of maximal absorption happens in the diffusive regime. We further study how the absorbed energy changes, depending on the geometrical parameters as well as the scattering properties of the random media. Strikingly, embedding the random medium into an open cavity increases the absorbed energy, providing 23-fold enhancement compared to the random medium without cavity. As a potential application, we theoretically demonstrate that random media can improve the absorption of light in existing light trapping systems by 2.2, thus demonstrating that the maximal absorption regime in random media is promising for light harvesting devices.

2. Methods

To simulate light propagation through a random medium, we use a probabilistic approach based on a Monte Carlo scheme, which we briefly describe here. A more complete treatment of this framework and its validation can be found elsewhere [58, 59]. The random medium consists of spherical scatterers with diameter d distributed homogeneously in an absorbing background. The simulation is performed on a finite volume of random medium with the form of a rectangular parallelepiped volume with a square basis, Fig. 1(a) inset. Incident light is launched though the central point of one of the surfaces at normal incidence unless stated otherwise. We use a wavepacket description of light instead of single photons in order to simulate absorption along the optical path. Between two successive scattering events the wavepacket travels in a straight line losing its energy through absorption in the background according to Beer-Lambert's law [60]. The mean free path of light l_{free} between two successive scattering events is determined as:

$$l_{free} = \frac{2d}{3FQ_{sca}}, \tag{1}$$

where $F = \pi d^3 C / 6$ is the filling factor, C the concentration of scatterers, Q_{sca} the scattering efficiency for each individual scatterer. The transport mean free path is determined as: $l^* = l_{free} / (1-g)$ with $g = \langle \cos\theta \rangle$ the average scattering angle or anisotropy parameter [61]. The

Optics EXPRESS

parameters Q_{sca} and g are calculated using Mie theory [59]. We assume that the interparticle distance p follows the random distribution expressed by: $p = -l_{free} \log \Sigma$, where Σ is sampled uniformly between 0 and 1. When a wavepacket experiences a scattering event from a particle, it changes its direction. The probability $q(\theta)$ of the wavepacket to be scattered at a given angle is calculated using the Henyey-Greenstein distribution [62]:

$$q(\theta) = \frac{1-g^2}{4\pi\left(1+g^2-2g\cos\theta\right)^{3/2}}. \quad (2)$$

The wavepackets are sequentially traced until they reach the box boundaries, where the directions and energies of such output wavepackets are recorded. The total initial energy of all wavepackets is set to unity for normalization purposes. To achieve a reasonable approximation of a realistic system, 10^8 wavepackets are launched for every simulation. The transmitted energy T (respectively, reflected energy R) is calculated as the total energy of wavepackets that exit the system with a zero or positive (respectively, negative) scalar product between their direction and the incident light direction. In this way, wavepackets that exit the side walls of the medium are also accounted for in the transmission or the reflection. Finally, the absorbed energy E_{abs} is calculated as the difference between incident energy and the sum of reflected and transmitted energies. The optical path of light (OPL) for transmitted OPL_T (respectively, reflected OPL_R) direction is calculated by taking the ratio of transmitted (respectively, reflected) light energy to the corresponding energy in the absence of the absorber T_0 (respectively, R_0) and utilizing Beer-Lambert's law: $OPL_T = -\log(T/T_0) / \alpha$, where α is the absorption coefficient and $OPL_R = -\log(R/R_0) / \alpha$. Unless otherwise stated, we use the following values for the simulation parameters: the spherical scatterers have a diameter d = 0.5 μm; the surrounding medium is a solution with refractive index n = 1.3 and absorption coefficient α = 30 m^{-1}; and the incident free-space wavelength is λ = 550 nm. We vary the refractive index of scatterers n between 1.6 and 2.6, which corresponds to commercially available polystyrene beads and titanium dioxide particles, respectively. We choose small values of α because higher values suppress multiscattering effects in random media as will be demonstrated in the text.

3. Results and discussions

3.1. Maximal absorption regime

To explain the maximal absorption regime in random media, we first introduce the known behavior for light reflection and transmission in random media [63]. As we increase the filling factor F of the random medium, OPL_T increases from being equal to the thickness of the medium L – horizontal dashed line in Fig. 1(a) – to much larger values corresponding to the multiscattering regime. However, for F > 1% (l_{free} < 10 μm) only a small part of the energy is transmitted in the forward direction, as indicated by the blue line in the inset of Fig. 1(b). Concurrently, OPL_R rises slightly at first due to the multiscattering, but decreases for F > 1% because the sample reflectivity increases. The nature of light propagation evolves from ballistic to highly scattering: according to Eq. (1), the mean free path l_{free} changes from several meters (for $F < 10^{-4\%}$) to less than micrometer (F > 10%).

In such a system, we find that the absorbed energy E_{abs} exhibits a non-monotonic dependence that peaks at F_{cri} = 1.3% corresponding to l_{free} = 7 μm, Fig. 1(b). This behavior is associated with different regimes of light propagation: weak (I), moderate (II) and strong (III), Fig. 1(c). In the weak scattering regime (F<<1%, l_{free} ~1 cm), most of the energy is transmitted in the forward direction along the path of incident light and, thus, E_{abs} grows with OPL_T. In the moderate or so-called diffusion regime, all photons lose their initial direction after travelling about 100 μm in the medium and spread over the entire absorber volume. In the strongly scattering regime (F>5%, l_{free} < 2 μm), the energy is mostly backreflected, so

Optics EXPRESS

that negligible amount of light reaches the distant parts of the absorber – black regions in the colormap, Fig. 1(cIII). In this case, E_{abs} follows the same trend as OPL_R, decreasing with increasing F. From the other perspective, our calculations confirm that optical absorption increases with l_{free} for strongly scattering media (regime III) [52]. Overall, although regime I is intuitive and regime III was studied in the context of random lasers, regime II, where maximal absorption occurs, was overlooked. Maximal absorption occurs when the number of scatterers is high enough that the incident light experiences multiscattering, but low enough that the light is not strongly confined and benefits from the full absorber volume.

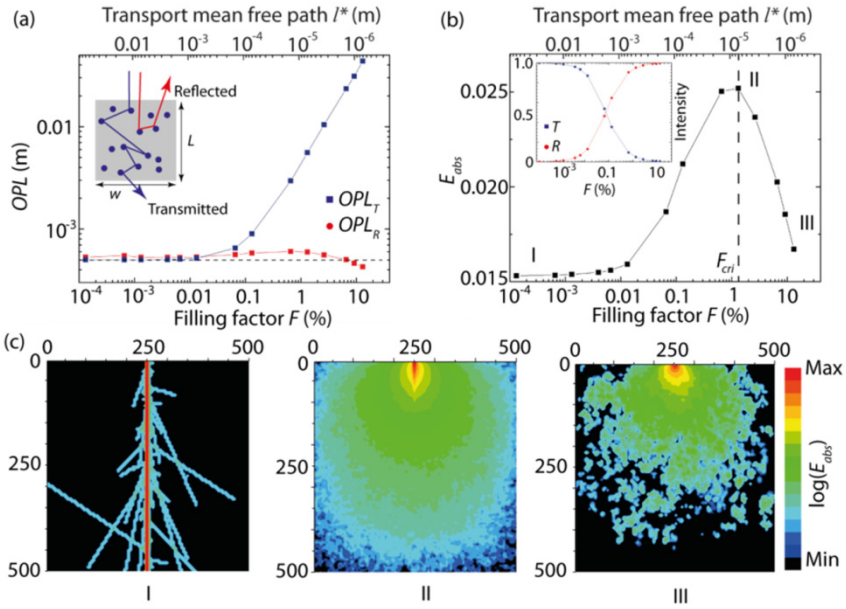

Fig. 1. Absorption in a random medium. (a) Optical transmitted and reflected path lengths OPL_T and OPL_R in a cubic random medium ($L \times w \times w$) with L = 500 μm and w = 500 μm composed of spherical scatterers (d = 0.5 μm, n = 2.6) in an absorbing background, as a function of the filling factor F. The dashed horizontal line corresponds to L. The inset shows the geometry under study. (b) Absorbed energy E_{abs} in the random medium as a function of the filling factor F. The inset shows the normalized transmitted T (dark blue) and reflected R (red) intensity of light. The dashed line corresponds to F_{cri} = 1.3%. (c) Logarithmic energy distribution of the light propagating in the central plane of the random medium described in (a) corresponding to (I) $F = 10^{-4\%}$, (II) F = 1%, and (III) F = 10%. The color scale is common to all three colormaps. All dimensions are given in micrometers.

3.2. Influence of geometrical parameters and scattering properties

Geometrical parameters and scattering properties of random media can be used to tune the light reflection and transmission, and consequently its absorption [14, 64]. Although light absorption in regimes I and III can be easily understood (as discussed below), the behavior of absorption in regime II is much less intuitive. In this section, we study how geometrical parameters and scattering properties influence the maximal absorbed energy and F_{cri}.

To study the first effect, we consider in Fig. 2(a) random media with various values for the width w, while keeping L constant at 500 μm. For $F < 10^{-3\%}$ (l_{free} ~1 cm), E_{abs} does not depend on w because light propagates mostly without scattering events, Fig. 2(a). Defining E_0 as the absorbed energy in the absence of scatterers $E_0 = E_{abs}(F \to 0)$, we observe that the presence of a random medium increases E_{abs} as compared to E_0 for $w > 250$ μm, Fig. 2(a). At the same time, for w = 250 μm and 100 μm, E_{abs} first decreases with increasing F and then reaches a local maximum. This is because for such small lateral dimensions, photons that undergo scattering events predominantly exit the system from the sides, resulting in a lower

Optics EXPRESS

OPL as compared to photons that propagate along the incident direction in the absence of random medium. With further increase of F, the emergence of multiscattering improves OPL and E_{abs} reaches a local maximum. However, for $F > 10\%$ ($l_{free} < 1$ μm), E_{abs} decreases in all cases because of the strong reflection. If w increases above 500 μm, the peak value of E_{abs} (which we call E_{max}) grows until it saturates for $w > 1000$ μm, implying that for very wide samples E_{abs} is limited not by the lateral confinement, but by the photons escaping through the top and bottom surfaces, Fig. 2(c). Therefore, for those parameters, the presence of a random medium improves E_{abs} as compared to E_0, only if $w \geq 0.8L$.

Next, we vary L while keeping a constant width $w = 500$ μm. Figure 2(b) shows that for $L = 100$ μm, 250 μm and 500 μm ($w \geq L$) E_{abs} follows a bell-shaped curve – for similar reasons as in Fig. 2(a). However, we observe a local minimum for $L = 750$ μm at $F = 0.1\%$, which resembles the E_{abs} behavior for $w < 250$ μm observed previously. For $L > 1000$ μm or $w \leq 0.8L$, the enhancement due to the presence of a random medium E_{max}/E_0 tends toward unity (with F_{cri} going to zero), demonstrating that increasing L is not beneficial without simultaneously increasing w, Fig. 2(d). If $L < 10$ μm the sample consists only of a few layers of scatterers and does not support multiscattering, therefore E_{max}/E_0 again goes to unity. We didn't observe a similar behavior for large w and $L = 500$ μm since in that case the medium was always in the multiscattering regime. The presence of a random medium brings maximum improvement (E_{max}/E_0 reaches its maximum value of 2.4) for a distance of L ~200 μm, which corresponds to w ~2.5L.

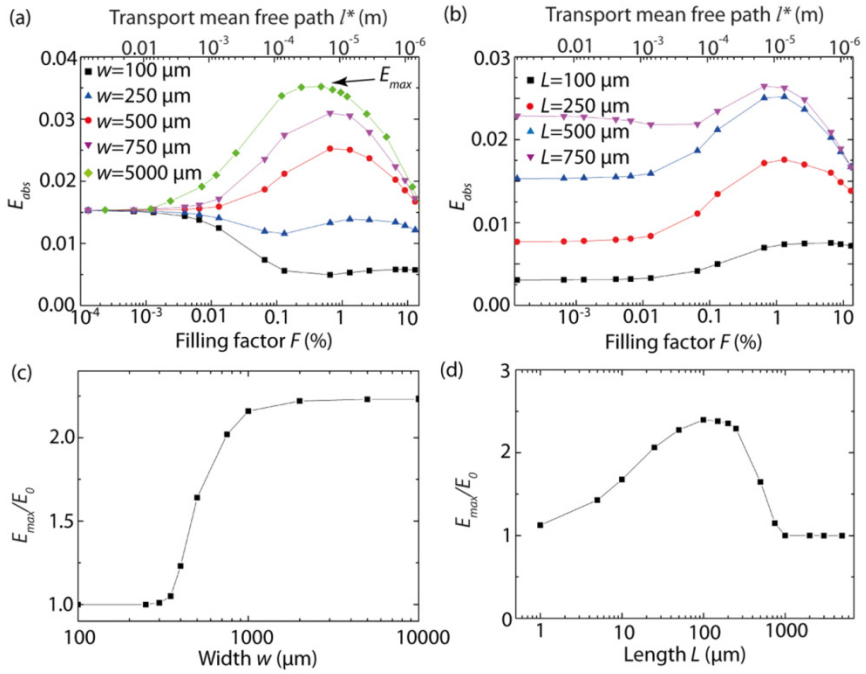

Fig. 2. Absorbed energy E_{abs} for a square prism with dimensions $L \times w \times w$ filled with a random medium when varying: (a) the width w ($L = 500$ μm, $d = 0.5$ μm, $n = 2.6$); (b) the length L ($w = 500$ μm, $d = 0.5$ μm, $n = 2.6$). (c) The maximum absorbed energy enhancement E_{max}/E_0 dependence on w for parameters as in (a). (d) The enhancement E_{max}/E_0 as a function of L for parameters as in (b).

Optics EXPRESS

Table 1. Properties of scatterers with different refractive index *n* and diameter *d*, and their effect on absorbed energy for a square prism with dimensions *L* × *w* × *w* (*L* = 500 μm).

n	d (μm)	g	Q_{sca}	w = 5000 μm			w = 500 μm		
				F_{cri} (%)	l^* (μm)	E_{max}	F_{cri} (%)	l^* (μm)	E_{max}
1.6	0.5	0.76	0.78	3.0	59.7	0.0364	5.2	34.6	0.0316
2.0	0.5	0.72	3.63	0.6	58.0	0.0362	1.1	30.0	0.0309
2.6	0.5	0.45	3.62	0.3	51.6	0.0352	1.3	12.9	0.0252
2.6	1	0.65	3.31	1.0	55.5	0.0359	3.8	15.3	0.0291
2.6	2	0.68	2.62	2.8	56.1	0.0359	6.9	23.2	0.0296

Let us now study the effect of the scatterer refractive index n and size d while the other parameters are kept fixed. Figures 3(a) and 3(b), respectively, depict E_{abs} as a function of F for selected values of n, respectively d. These parameters affect the values of Q_{sca} and g for individual scatterers as shown in Table 1. While all E_{abs} curves have similar shapes, the values for F_{cri} and E_{max} differ. The difference in E_{max} becomes even more pronounced for smaller w; for example, E_{max} reaches 3% for d = 2 μm while it is only 2.5% for d = 0.5 μm, Fig. 3(c). Furthermore, notice how media with scatterers that have similar g (n = 1.6 and 2.0) or Q_{sca} (n = 2.0 and 2.6) still have different F_{cri}. In Table 1, we observe that the main parameter determining light transport in the random medium, l^*, shows almost identical values at F_{cri} for the different scatterers. Furthermore, from the same table we find that values of E_{max} correlate well with that of g, which we explain further in the text.

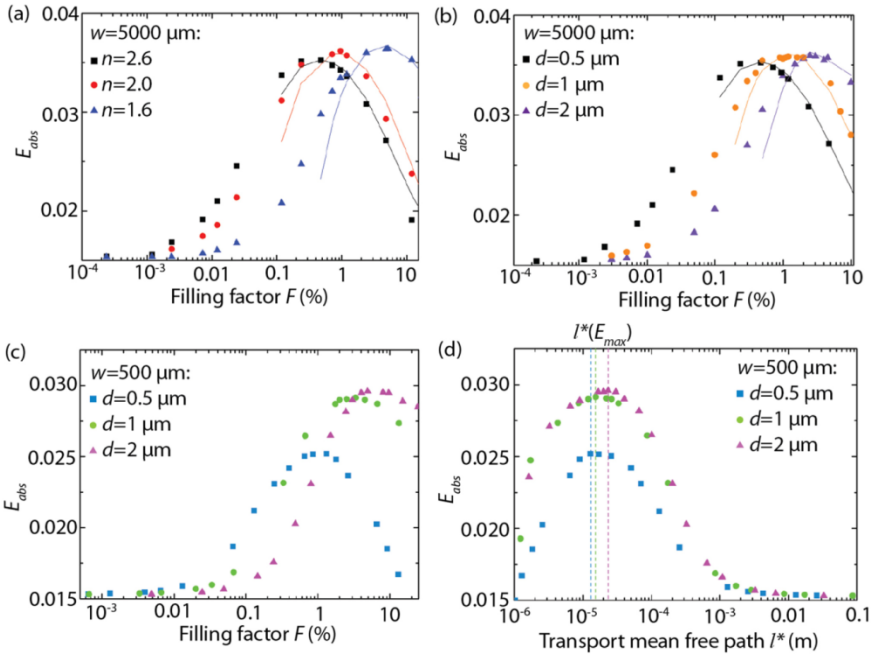

Fig. 3. Absorbed energy E_{abs} for a square prism with dimensions $L \times w \times w$ (L = 500 μm) filled with a random medium when varying: (a) the refractive index n (w = 5000 μm, d = 0.5 μm); (b,c,d) the scatterers diameter d (n = 2.6; w = 5000 μm in (b) and w = 500 μm in (c) and (d)). Points refer to Monte Carlo simulations, and lines to the analytical diffusion model based on Eq. (3). The same data are plotted against the filling factor (c) and the transport mean free path (d).

Optics EXPRESS

3.3. Analytical model based on diffusion approximation

To explain the difference in E_{max} for different scatterers, we use a solution of the light diffusion equation for an infinitely wide slab with thickness L [63]. The expression for E_{abs} is given by the following formula:

$$E_{abs} = 1 - \frac{1}{2}\sum_{m=-\infty}^{\infty} \{\mathrm{sgn}(z_{1,m})\exp(-\sqrt{\frac{3\alpha}{l^*}}|z_{1,m}|) - \mathrm{sgn}(z_{2,m})\exp(-\sqrt{\frac{3\alpha}{l^*}}|z_{2,m}|) - \mathrm{sgn}(z_{3,m})\exp(-\sqrt{\frac{3\alpha}{l^*}}|z_{3,m}|) + \mathrm{sgn}(z_{4,m})\exp(-\sqrt{\frac{3\alpha}{l^*}}|z_{4,m}|)\}, \quad (3)$$

where $\mathrm{sgn}(x) = -1$ if $x < 0$ and $\mathrm{sgn}(x) = 1$ if $x > 0$; $z_{x,m}$ ($x = 1..4$) are the distances defined as follows:

$$\begin{cases} z_{1,m} = L(1-2m) - 4mz_e - z_0 \\ z_{2,m} = L(1-2m) - (4m-2)z_e + z_0 \\ z_{3,m} = -2mL - 4mz_e - z_0 \\ z_{4,m} = -2mL - (4m-2)z_e + z_0 \end{cases}, \quad (4)$$

where $z_0 = l^*$, $z_e = 2Al^*/3$ and A is a parameter that characterizes reflection of light at the interface to fulfill the boundary conditions for diffusion:

$$A = \frac{1 + 3\int_0^{\pi/2} R(\theta_i)\cos^2(\theta_i)\sin(\theta_i)d\theta}{1 - 2\int_0^{\pi/2} R(\theta_i)\cos(\theta_i)\sin(\theta_i)d\theta}, \quad (5)$$

where $R(\theta_i)$ is the Fresnel reflection coefficient for light with incident angle θ_i at the surface of the random medium.

The results obtained with the diffusion approximation Eqs. (3)–(5) are shown as solid lines in Figs. 3(a) and 3(b) and compared with Monte Carlo simulations for a very wide slab – in our case we choose w = 5000 μm since E_{max} does not change significantly above this value, Fig. 2(c). For $F > 0.1\%$ ($l_{free} < 100$ μm) we find excellent agreement between the two methods, Figs. 3(a) and 3(b). For smaller values of F the diffusion approximation does not hold because l^* becomes comparable with L meaning that in this regime the light propagation is not completely randomized. Thus, the diffusion approximation can be used as a fast and precise method to determine F_{cri} for maximal absorption. From Eq. (3) it can be concluded that for a given α, L and one type of scatterers (with given n and d), E_{abs} reaches a maximum for specific $l^*(E_{max})$, which can be found numerically. Interestingly, from Table 1 it can be seen that $l^*(E_{max})$ varies only slightly for different scatterers when w = 5000 μm. Therefore, for wide slabs $l^*(E_{max})$ – of one type of scatterers – can used as an approximate value of $l^*(E_{max})$ for another scatterers. This provides a simple design rule to find an approximate value of F_{cri} and to optimize the absorption. Slight differences in l^* for different scatterers are caused by small variations in A (numerical calculations using Eq. (5) show typical values of $A(E_{max})$ between 1.05 and 1.12). The difference of $l^*(E_{max})$ for different types of scatterers is more pronounced for the narrower cavity, w = 500 μm. However, a constant l^* still provides a good approximation, Fig. 3(d). For example, scatterers with d = 0.5 μm and n = 1.6 reach E_{max} at l^* = 34.6 μm while scatterers with the same d and n = 2.6 have $l^*(E_{max})$ = 12.9 μm. Numerical calculations show that $E_{abs}(l^*$ = 34.6 μm) = 0.242 for n = 2.6, which corresponds to more than 90% of E_{max} (= 0.0255). Similar results are valid for other combinations of n

Optics EXPRESS

and d and for $w > 500$ μm (data not shown). The approximation $l^* = const$ breaks for smaller w because light escaping by the side walls becomes significant.

For $l^* << L$ (in our case for $l^* < 5 \times 10^{-5}$ μm), all exponents in Eq. (3) that contain L will cancel each other, simplifying the expression to:

$$E_{abs} \approx 1 - \frac{1}{2}\exp(-\sqrt{3\alpha l^*}) - \frac{1}{2}\exp[-\sqrt{\frac{3\alpha}{l^*}}(l^* + \frac{4}{3}Al^*)]. \quad (6)$$

Thus, E_{abs} increases with A. As evident from Eq. (5), A is determined by $R(\theta_i)$. Numerically $R(\theta_i)$ is calculated using an effective refractive index of the random medium [63]. Physically, reflection at the interface is caused by the light scattering from spheres located in the surface layer of thickness b. Thus, semi-qualitatively we can relate the reflection coefficient to the total scattering efficiency of this surface layer. In certain area A and thickness b, there is CAb scatterers. The probability of light being scattered in this layer is: $CAbQ_{sca}d^2/(4A)$. The reflectivity R is then proportional to this probability:

$$R \sim \frac{CQ_{sca}\pi d^2 b}{4} = \frac{6FbQ_{sca}\pi d^2}{4\pi d^3} = \frac{3}{2}\frac{bFQ_{sca}}{d} = \frac{b}{l^*(1-g)}. \quad (7)$$

From Eqs. (5) and (7), we expect strong dependence of A on g. Indeed, numerical values for Eq. (5) show that $A(g)$ grows with g for a constant l^* (data not shown). It follows from Eq. (6) that $E_{abs}(g + \Delta g, l^*) > E_{abs}(g, l^*)$ and, in turn, $E_{max}(g + \Delta g) > E_{max}(g)$. Hence E_{max} increases with g, which we indeed observe in Table 1. This simple design rule predicts that scatterers with higher g will show higher E_{max}. This is an important result since g goes to unity when n decreases, thus we can use scatterers with low n to achieve high E_{max} values. However, if g approaches unity, we have to increase F to infinity in order to reach the $l^* = const$ condition discussed in the previous paragraph. Since F is limited to values of 50-70% for closed packed systems, it sets the upper limit for the maximal value of g and, in turn, E_{max}. Moreover, our formalism breaks down for high values of F ($F > 20\%$, $l_{free} < 0.5$ μm) when short-range order and near-field effects have to be taken into account [65]. The maximal absorbed energy E_{max} also grows with g for finite w (Table 1). Indeed, the relation $E_{abs}(g + \Delta g, l^*) > E_{abs}(g, l^*)$ is clearly visible in Fig. 3(d). This comes as no surprise since the expression for E_{abs} for finite w has a similar structure as Eq. (3) [66]. Finally, we would like to stress that in order to point out interesting design rules, we only semi-qualitatively explain tendencies observed in numerical simulations, leaving rigorous proofs beyond the scope of this paper.

3.4. Random medium in an open cavity

To increase the absorbed energy in the random medium, we now embed it into an open fully reflective cavity, which contains two square openings with dimensions $s \times s$: one at the center of the top and one at the center of the bottom face, for the reflected and transmitted light, see the inset in Fig. 4(a). We demonstrate that the regime of maximal absorption is also present in such hybrid system. We choose such a configuration to compare the performances of the random medium in an open cavity (henceforth referred to as the open cavity) to that of the random medium without reflective walls with exactly the same geometry (henceforth referred to as the free random medium). Additionally, we introduce different enhancement factors k to quantify the enhancement provided by the open cavity.

The open cavity configuration leads to an increase in the effective volume which, in turn, enhances OPLs. For instance, OPL_R increases by a factor $k_R = 32$ for low F compared to the free random medium, Figs. 4(a) and 4(b). The OPL_T enhancement, k_T reaches a maximum of 27 at the critical filling factor $F_{cri} = 0.07\%$ and then drops along with OPL_R. This is because for $F > 1\%$ ($l_{free} < 10$ μm) most of the light is confined in a volume smaller than the size of the cavity; hence very little is reflected from the walls leading to the decrease of the

Optics EXPRESS

enhancement factors k to unity, Fig. 4(b). The energy absorption E_{abs} peaks at F_{cri} = 0.13%, with an enhancement k_E = 23 for the absorbed energy compared to the free random medium, Figs. 4(c) and 4(d). The fact that the maximum energy absorption occurs at different filling factors for the free random medium and for the open cavity is caused by the different effective volumes for these two geometries. To visualize the absorption in the cavity, in Fig. 4(e) we plot the light intensity in the central plane of the cavity with the same color scale as in Fig. 1(c). The second diagram illustrates the maximum of the absorbed energy, whereas the third diagram shows strong backreflections corresponding to high F values.

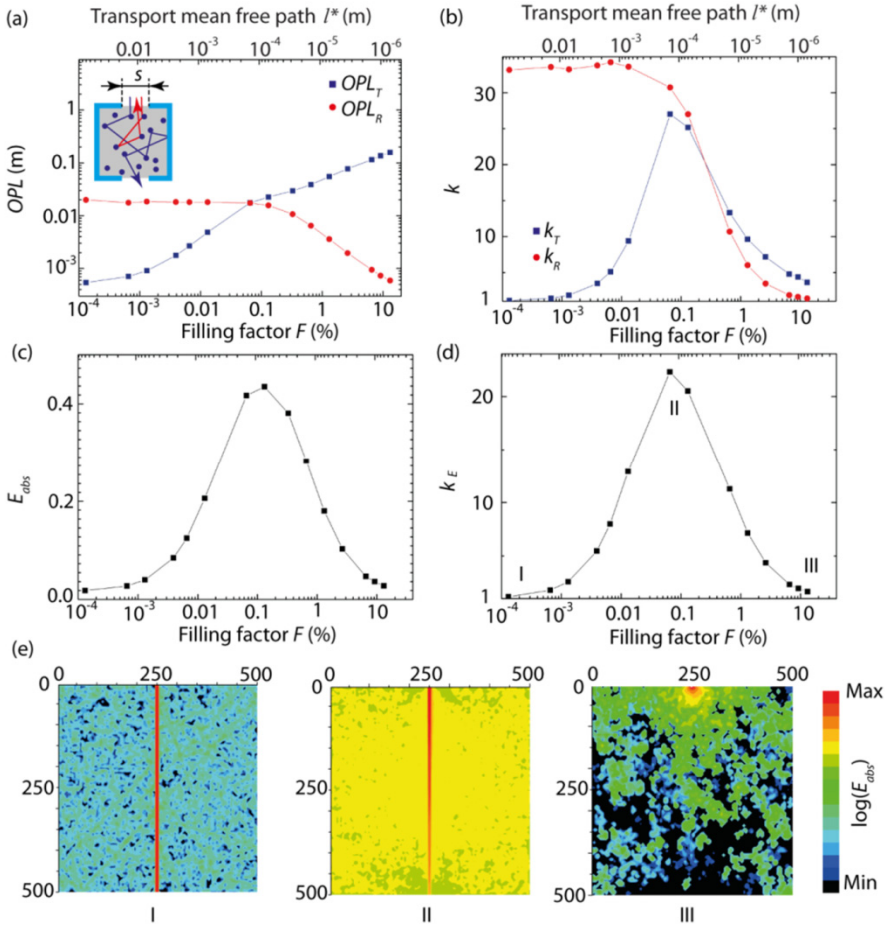

Fig. 4. Absorption in a random medium (d = 0.5 μm, n = 2.6) surrounded by a fully reflective cavity (L = w = 500 μm) containing two square openings with size s = 100 μm. (a) OPL_T and OPL_R. The inset shows a schematic of the geometry. (b) OPL enhancements compared to the free random medium k_T and k_R. (c) E_{abs} in the medium. (d) Enhancement of the absorbed energy compared to the free random medium k_E. (e) Logarithmic intensity distribution of light propagating in the central plane corresponding to (I) $F = 10^{-4\%}$, (II) F = 0.05%, (III) F = 10%. The color scale is common for all three colormaps. The dimensions are given in micrometers.

Let us now study the influence on light absorption of various parameters describing the random medium in the open cavity. The probability of light escaping from the open cavity is given by the ratio of the openings area to the total cavity area. This is demonstrated by changing w while keeping s fixed: E_{abs} changes, but retains a bell-shaped profile for all w, in contrast to the free random medium, compare Figs. 2(a) and 5(a). Similarly, the light confinement changes with s, leading to different E_{abs}, Fig. 5(b). By reducing s to 5 μm, we

Optics EXPRESS

can achieve absorption of 99% simply due to the high confinement of the cavity. Similar to the free random medium, the filling factor F_{cri} producing the largest absorption shifts when the refractive index n of the scatterers changes; for the three different indices investigated in Fig. 5(c), we observe that l_{free} at F_{cri} is close to 132 μm, which is about nineteen times larger than in the case of the free random medium. Furthermore, in contrast to the free random medium, now the E_{max} values remain similar for the different refractive indices. This is caused by the reflective walls, which now play the major role, rather than l^*, for confining the light, as is evident from the 23-fold enhancement observed for E_{abs} in Fig. 4(d).

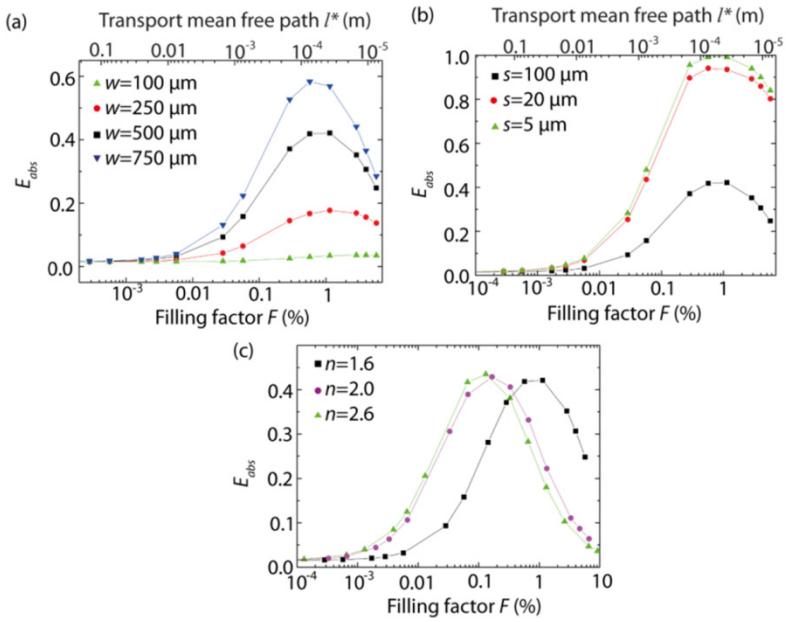

Fig. 5. Absorbed energy E_{abs} for a random medium (d = 0.5 μm) surrounded by a fully reflective cavity (L = 500 μm) containing two square openings with size s– see Fig. 4(a) inset – as a function of: (a) the cavity width w (s = 100 μm, n = 1.6), (b) the openings size s (w = 500 μm, n = 1.6) and (c) the refractive index n of the scatterers (s = 100 μm, w = 500 μm).

3.5. From weak to strong absorbers

Different light trajectories have different OPLs in the random medium. With the presence of the absorber, the energy transmitted through the system for a given trajectory is modified according to Beer-Lambert's law [60]. The trajectories with longer OPL undergo stronger absorption. As a result, the nature of light propagation also depends on the value of the absorption α: while for weak absorbers it is diffusion-like, it becomes dominantly ballistic for strong absorbers, reducing multiscattering effects [42]. In the latter case, Fig. 6 shows that E_{max}/E_0 decreases to unity for $\alpha > 10^4$ m^{-1}, meaning that the benefits of multiscattering are then lost.

To characterize the effect of absorption in the medium, we introduce the absorption mean free path l_{abs} that can be related to l^* and to the inelastic mean free path l_i, which is defined as the travelled length over which the light intensity is reduced by a factor $1/e$ due to absorption ($l_i = 1/\alpha$); l_{abs} is then defined as the average distance between begin and end points for paths of length l_i [4]:

$$l_{abs} = \sqrt{\frac{1}{3} l_i l^*} = \sqrt{\frac{l^*}{3\alpha}}. \quad (8)$$

Optics EXPRESS

The parameter l_{abs} reflects the nature of light propagation in random media with gain or losses [6]. Till now, we considered a case of weak absorption, meaning that l_i was larger than L. As absorption increases, l_i becomes smaller and smaller, meaning that light will be absorbed even with ballistic propagation over the length of L. In this case, introduction of random media becomes disadvantageous as it only brings unnecessary reflection losses, as indicated by the dark blue line in Fig. 6. In general, the effect of absorption on light propagation in random media is not novel [42], but the behavior of the absorbed energy peak requires special attention. As we increase the absorption α in the background, F_{cri} decreases, as indicated by the dashed line in the inset of Fig. 6(a). This line follows the position of the E_{abs} maximum (corresponding to F_{cri}). This shift is less pronounced for the open cavity since the light confinement in that geometry is dominated by the reflective walls (for $F > 10\%$) and, thus, weakly depends on l_{abs}, Fig. 6(b).

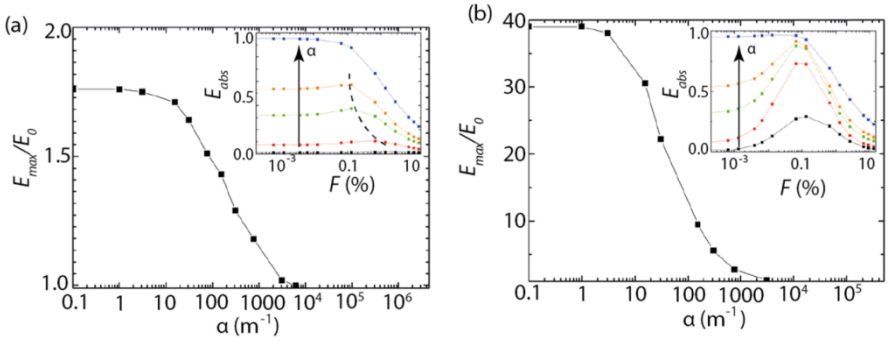

Fig. 6. Dependence of E_{max}/E_0 on the absorption coefficient α for: (a) a free random medium (L = 500 μm, w = 500 μm, d = 0.5 μm, n = 2.6); (b) an open cavity with the same parameters as in (a) and s = 100 μm. The insets show E_{abs} for the respective geometries at α = 30 m^{-1} (black), 150 m^{-1} (red), 750 m^{-1} (green), 1500 m^{-1} (orange) and 6000 m^{-1} (dark blue).

3.6. Improving light trapping for solar cells

To illustrate an application of maximal absorption, we now consider the optimization of the light trapping system shown in Fig. 7(a). Using such a device for thin solar cells, Tvingstedt *et al.* demonstrated a 25% increase in the absorption of the solar cell and photocurrent [24]. Additionally, such a system demonstrates that the regime of maximal absorption is also present in the buried absorber system, i.e. where absorption happens only in some parts of the random medium as explained below. The proposed geometry includes highly reflective mirrors with light trapped in the space between them. The absorption happens only in the thin layer (50 nm) of active material with the absorption coefficient $\alpha = 10^5$ m^{-1}, while all the remaining material is non-absorbing. A concentrator focuses all the light reaching its surface into the opening in the top mirror. Here, an array of glass lenses with focal distance f = 1 mm acts as concentrator [24]. The choice of lens material and the quality of fabrication constrain the value of f for a given w [67]. The cone of light entering the solar cell covers a range of incident angles between β = 0 and β = 14° for w = 500 μm. Such a low β does not allow the solar cell to efficiently trap light inside, since the incident light is just reflected back by the structure. To overcome this limitation, we introduce a random medium in the space between the top mirror and the active layer. To simulate the light behavior in this device, a truncated unit cell with reflective side walls is considered, Fig. 7(b).

Quite strikingly, an appropriate concentration of scatterers confines light inside the structure – even for low illumination angles β – and enhances absorption inside the active layer, Fig. 7(c). For instance, even for β = 0° (corresponding to light incident normally on the structure), the E_{max}/E_0 ratio reaches 55. Whereas for light incident at β = 0° and 8°, E_{abs} peaks at F = 0.5% (l_{free} = 19 μm) showing similar values of E_{max} in both cases; for β = 15°, E_{abs}

Optics EXPRESS

dependence is much broader with a peak at $F = 0.025\%$ ($l_{free} = 380$ μm). The latter effect is due to the different effective geometry that light experiences at a given angle as compared to β = 0° case. To summarize the angular performance of the light trapping scheme in the presence of a random media, we show in Fig. 7(d) the absorbed energy E_{abs} for different angles. For β < 8°, the incident light is reflected from the bottom mirror and exits through the same opening as entered, not being absorbed significantly, while for higher β light is efficiently confined inside the cell. This is why there is a jump in E_{abs} at β = 8° in the absence of scatterers. On the other hand, for $F = 0.5\%$ E_{abs} shows a weak dependence on β since light experiences strong multiscattering. Therefore, light absorption significantly improves in the presence of random medium for angles β < 8°. Considering the total angular range of β = 0 – 14°, we observe a 2.2 enhancement of E_{abs} for $F = 0.5\%$ and 1.4 for $F = 0.025\%$ as compared to the case without scatterers. Furthermore, the proposed multiscattering phenomenon is non-resonant and hence broadband, which is important when working with solar energy. Although light trapping is more efficient with smaller s, larger values of s provide robustness and tolerance for the alignment of the solar concentrator with respect to the incident light [26], e.g. for the solar concentrator in Fig. 7 this tolerance is only 2.9°.

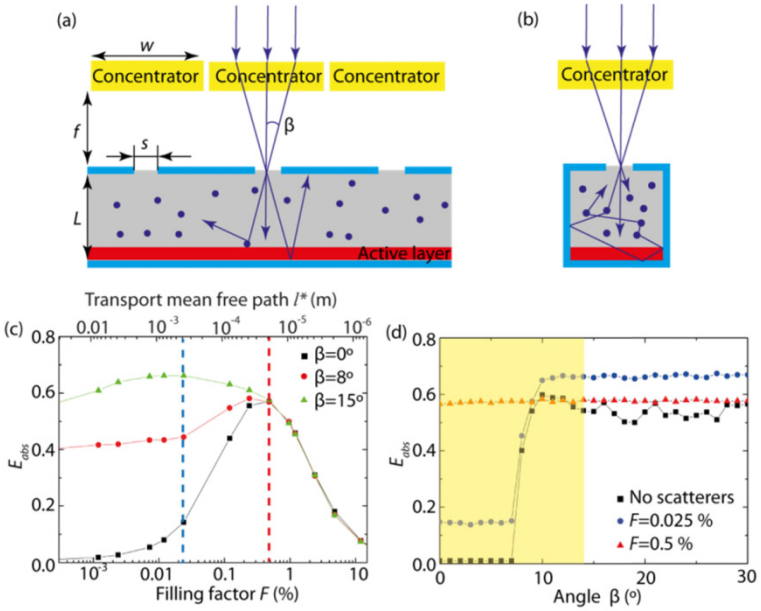

Fig. 7. (a) Schematic of light trapping device with two reflective surfaces, active photovoltaic layer (in red) and an array of concentrators on top. (b) Schematic of the truncated unit cell used in the numerical simulations. (c) E_{abs} as a function of F for light entering the opening at different angles in the presence of a random medium ($d = 0.5$ μm, $n = 2.6$, $L = 100$ μm, $w = 500$ μm, $s = 50$ μm). The blue dashed line corresponds to $F = 0.025\%$ and the red one to $F = 0.5\%$. (d) E_{abs} as a function of β; the yellow area corresponds to β = 0 – 14°, the angular range of light after it has passed through a concentrator with $f = 1$ mm.

4. Summary

We have shown that the maximal absorption regime for a random medium corresponds to the conditions for diffusion-like energy transport: the filling factor F has to be high enough to sustain multiscattering in the medium and, at the same time, low enough to allow light to penetrate inside the material. We identified design rules for geometries where the introduction of a random medium becomes beneficial in terms of absorbed energy. The filling factor F_{cri} which maximizes light absorption depends on the relation between the transport mean free path of light l^* and the geometrical size of the medium. Moreover, l^* remains almost constant

Optics EXPRESS

for different scatterers. The maximal absorbed energy E_{max} increases with the asymmetry parameter g. Typical values of F_{cri} are in the range from 0.5% to 10% (the corresponding mean free path values range from 7 to 132 μm).

The amount of absorbed energy can be further increased (from 1.7 to 23-fold) by introducing a hybrid system: an open cavity around the random medium. Such hybrid system has an advantage over an open cavity because the absorption enhancement is alignment-free; and over the random medium because the value of the enhancement is higher. Furthermore, the enhancement provided by the scattering medium decreases as the absorption α grows, because the nature of light propagation changes from diffuse to ballistic. The application of these principles to absorption for a photovoltaic system has been illustrated by demonstrating a 2.2 absorption enhancement when introducing a random medium with appropriate filling factor in the system. The combination of an open reflective cavity with a random medium ensures strong photon confinement, with the additional benefits of wide-angled and broadband operation. This approach is promising for improving the efficiency of solar cells, decreasing lasing threshold in random lasers as well as for sensing applications where the optical absorption of minute quantities of analyte must be detected.

Funding

Swiss National Science Foundation (406440-131280/1).

Acknowledgements

It is a pleasure to acknowledge stimulating discussions with Dr. T. V. Raziman.